Science of the Total Environment 685 (2019) 856–866

Contents lists available at ScienceDirect

Science of the Total Environment

journal homepage: www.elsevier.com/locate/scitotenv

Modelling oil trajectories and potentially contaminated areas from the *Sanchi* oil spill

Fangli Qiao [a,b,c,*], Guansuo Wang [a,b,c], Liping Yin [a,b,c], Kan Zeng [b,d], Yuanling Zhang [a,b,c,e], Min Zhang [a,b,c,e], Bin Xiao [a,b,c], Shumin Jiang [a,b,c,e], Haibo Chen [f], Ge Chen [b,d]

[a] First Institute of Oceanography, Ministry of Natural Resources, Qingdao, China
[b] Laboratory for Regional Oceanography and Numerical Modeling, Qingdao National Laboratory for Marine Science and Technology, Qingdao, China
[c] Key Laboratory of Marine Science and Numerical Modeling (MASNUM), Ministry of Natural Resources, Qingdao, China
[d] College of Information Science and Engineering, Ocean University of China, Qingdao, China
[e] Key Laboratory of Data Analysis and Applications, Ministry of Natural Resources, Qingdao, China
[f] Key Laboratory of Ocean Circulation and Waves, Institute of Oceanology, Chinese Academy of Sciences, Qingdao, China

HIGHLIGHTS

- A comprehensive three-dimensional oil spill model is established.
- The potential polluted areas depended on the released oil properties.
- The leaked bunker oil expands into the Ryukyu island chain.

GRAPHICAL ABSTRACT

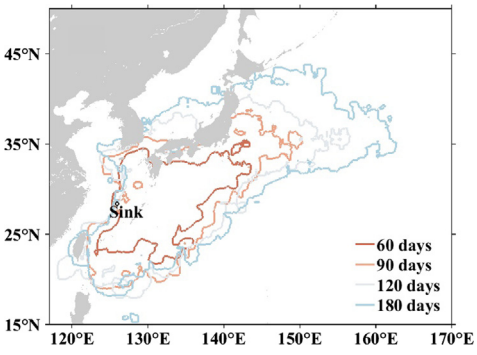

ARTICLE INFO

Article history:
Received 7 January 2019
Received in revised form 13 June 2019
Accepted 16 June 2019
Available online 19 June 2019

Editor: Ashantha Goonetilleke

Keywords:
Sanchi oil spill
Oil particles
Three-dimensional oil spill modeling
Lagrangian trajectory
Pollution probability

ABSTRACT

Oil spills are major threats to marine ecosystems. Here, we establish a three-dimensional oil spill model to simulate and project the short- and long-term trajectories of oil slicks and oil-contaminated water that leaked from the *Sanchi* wreckage. The pollution probability in surrounding areas for the period up to 180 days after the *Sanchi* sank is statistically analysed. The short-term simulations are consistent with synchronous SAR images and observational reports. The potentially polluted areas depend on the properties of the released oil. The coastal areas most likely to be affected by the bunker oil are located in the Ryukyu Island Chain, Tsushima Strait, on the south and east coasts of Japan. Approximately 50% to 70% of oil particles remain in the ocean and mainly expand along the Ryukyu Island Chain and the region southeast of the *Sanchi* wreck. Subsurface oil-contaminated water is likely to enter the Sea of Japan along the Tsushima Strait. Due to the rapid evaporation rate of condensate oil, the potentially polluted area is confined to regions within a 100 × 100 km area around the location of the shipwreck, and the contaminated region is closely associated with the surface wind.

* Corresponding author at: First Institute of Oceanography, Ministry of Natural Resources, Qingdao, China.
E-mail address: qiaofl@fio.org.cn (F. Qiao).

https://doi.org/10.1016/j.scitotenv.2019.06.255

1. Introduction

At 7:51 pm CST (China Standard Time or Beijing Time, GMT + 8 h) on 6 January 2018, the Panamanian-flagged, Iranian-owned oil tanker *Sanchi* that was carrying a full cargo of 136,000 metric tons of natural gas condensate, collided with the Hong Kong-flagged cargo ship CF *Crystal* in the East China Sea at (30°42′N, 124°56′E), 300 km from Shanghai, China (Yin et al., 2018; Sun et al., 2018; Lockwood, 2018; Carswell, 2018). The *Sanchi* caught fire after the collision, drifted for about 8 days on the sea surface, and eventually sank to a depth of 115 m at ~3 p.m. CST on 14 January 2018, in close proximity to the strong Kuroshio current (28°22′N, 125°55′E). Much of the leaked condensate is likely to have evaporated and burned before the *Sanchi* sank. However, the condensate oil remaining in the wreckage and the ship's own fuel (bunker oil, a heavier form of fuel oil, approximately 2000 tons) pose a threat to marine wildlife and ecosystems. Oil contamination may affect the ocean environment for several years (Kingston, 2002); in addition, clean-up of these substances becomes more complex after a vessel sinks (Lee et al., 1981). The oil-contaminated water, which contains compounds such as sulphides derived from the condensate (Aali and Rahmani, 2012), is expected to have a dramatic impact on marine ecosystems, affecting a broad range of species over the short and long term in the surrounding seas and even the open ocean (Peterson et al., 2003; Alonso-Alvarez et al., 2007).

Advection, or the drifting of oil on the sea surface, is the result of the combined actions of wind, ocean currents and surface waves (Schwartzberg, 1971). The presence of oil can also affect wind stresses, ocean surface waves and current systems (Cox et al., 2017). Ocean current systems around the shipwreck location are complex, comprising a seasonal wind-driven current in the upper ocean, the Tsushima Current, the strong western boundary Kuroshio Current, and small and mesoscale eddies (Guo et al., 2006). Numerical simulations of the current and thermal structure in the upper ocean would thus be helpful for oil spill projections. Trajectory models of oil spill movement that consider winds, ocean currents and tides are by far the best option for a quick response to oil spill events (Toz and Koseoglu, 2018). The Lagrangian method is more appropriate and displays greater efficiency in predicting real oil spill cases than the Eulerian approach (Delgado et al., 2006). With the Lagrangian method, the spatiotemporal distribution of oil droplets, slicks and oil-contaminated water can be characterised by the motion of virtual oil particles on the sea surface or underwater, and this method has been successfully applied to produce two-dimensional (2D) and three-dimensional (3D) oil spill models (Lonin, 1999; De Dominicis et al., 2013a, 2013b).

Researchers from the National Oceanography Centre (NOC), Southampton, UK, and the State Oceanic Administration (SOA), China, produced a map of potentially contaminated areas (NOC, 2018a; Yin et al., 2018; Carswell, 2018). The numerical simulations performed by the NOC and SOA are based on a high-resolution global ocean general circulation model (NEMO) (Madec, 2012) and an operational surface wave-tide-circulation coupled forecasting system (OFS) (Wang et al., 2016), respectively. The results of these two models confirm that oil-contaminated water was likely to reach southeastern Japan and the North Pacific along the strong Kuroshio current, and the remainder was likely to enter the Sea of Japan through the Tsushima Strait. Based on recent but unconfirmed information that *Sanchi* oil arrived at the island of Amami Ōshima (NOC, 2018a), the NOC updated their projections that the contamination could reach the Ryukyu Island Chain and potentially affect nearby coral reefs (NOC, 2018b).

The fates of oil spilled into the sea are diverse. Most of the oil spilled in the water will float on the surface and spread as slicks. In oil slicks with a high proportion of volatile components, the volume of these components quickly reduces by evaporation (Shen and Yapa, 1988). Under the effects of turbulence and surface waves, the surface oil breaks into tiny droplets and mixes with the water column. Some light hydrocarbons and polar components may dissolve and be retained in the water column until they are degraded, whereas heavy crude and residual oils will emulsify. These emulsions may persist on the water surface if they do not beach. In addition, the leaked oil may sink to the seabed along with the clay or sand (Shen and Yapa, 1988; Kingston, 2002). However, condensate oil has a volatile nature that differs markedly from that of traditional crude and residual oil, and this is the first time that it released in the ocean in such massive quantities. In addition, the unknown duration of the oil leakage after the *Sanchi* sank has led to great uncertainties in model projections.

Various numerical models have been developed to simulate oil transport and the fate of oil spills for specific ocean regions or events, such as the fast response 2D- and 3D-GNOME (General NOAA Operational Modeling Environment) (Zelenke et al., 2012), the 3D Oil Spill Model and Response System OILMAP (ASA, 1997), the operational system METEO-MOHID for the Prestige-Nassau oil spill (Carracedo et al., 2006), OILTRANS for the Northwest European continental shelf (Berry et al., 2012), and MEDSLIK-II (De Dominicis et al., 2013a, 2013b; Lardner and Zodiatis, 2017) for short-term oil fate forecasting in the Mediterranean Sea. The comprehensive 3D oil spill model consists of a group of algorithms that predict the fate and transport of spilled oil by simulating the processes of advection, diffusion, surface spreading, vertical mechanical dispersion, evaporation, emulsification and stranding (Cekirge et al., 1995). The drifting of oil particles is driven mainly by winds and ocean currents, so an accurate prediction of the dispersion of spilled oil strongly depends on ocean circulation and surface waves (Toz and Koseoglu, 2018).

Different with previous studies, the *Sanchi* event is special for both bunker and condensate oil leaked synchronously at subsurface water with complex oceanic circulations. Due to the unreleased reports that the oil leaked for at least 20 days, our study aims to set up a coupled three-dimensional oil spill model and focus on long-term simulations to give a maximum pollution maps with pollution probability analysis for the oil slicks and oil-contaminated water leaking from the *Sanchi* wreck. Various scenarios that consider oil properties and different emission periods are performed to produce pollution probability maps that show the risk of oil pollutants reaching particular areas of the ocean. A detailed discussion of the uncertainties is then provided.

2. Methods

The fate of spilled oil in water is governed by complex interactions of physical, chemical and biological processes, which are determined by the ambient marine environment and oil properties (Shen and Yapa, 1988). In this study, a coupled 3D model is established to provide short- and long-term simulations and projections for the *Sanchi* oil spill. This coupled 3D model has two parts: (1) a coupled 3D operational ocean forecast system (OFS) to simulate ocean environments, and (2) a 3D oil spill model to simulate the trajectories of oil particles based on their properties.

2.1. Operational ocean forecast system

The surface wave-tide-circulation coupled OFS has three components: the POM (Princeton Ocean Model) ocean circulation model, the MASNUM (Laboratory of Marine Sciences and Numerical Modeling of SOA of China) surface wave model and the tidal model. The wave model is coupled with the ocean circulation model using nonbreaking surface wave-induced mixing theory (Bv) (Qiao et al., 2004). Three models with different resolutions (quasi-global, northwest Pacific and coastal) are embedded and run simultaneously in the system. The high-resolution models are nested within the low-resolution models and receive open boundary conditions from them. The detailed model grid configurations are shown in Table S1, and the detailed model computational parameters were given in Wang et al. (2016). The system has already been successfully used to project the drift characteristics of *Ulva prolifera* in the Yellow Sea in 2008 (Qiao et al., 2011a) and regions

affected by nuclear radiation from the Fukushima nuclear power plant (Qiao et al., 2011b). The OFS outputs ocean currents, temperature, surface wave parameters and wind fields with an archived 3-h time step.

The circulation model, which is driven by the atmospheric model (MM5 for the regional model and Global Forecast System model for the global one) via surface forcing (surface wind and heat flux) (Zheng et al., 2012), provides the ocean currents and temperature for the oil spill model. The tidal current is coupled with the circulation model via tidal elevation as open boundary conditions (Wang et al., 2016). To provide a hot start for the new operational forecast run, the blended daily high-resolution sea surface temperature (SST) (available from the North-East Asian Regional project of the Global Ocean Observing System), sea level anomalies, Argo temperature and salinity profiles are assimilated into the model using the ensemble adjustment Kalman filter (EAKF) scheme (Yin et al., 2010).

The MASNUM wave model provides wave parameters for the oil spill model to compute the Stokes drift (Yuan and Hua, 1991; Yang et al., 2005). The model solves the energy balance equation and its complicated characteristic equations in wave-number space using spherical coordinates. As surface waves are dominant in the upper ocean (Lee et al., 2006), it is important to consider them in the coupled spill model, not only for a better simulation of the ocean surface temperature and current (Qiao et al., 2004; Qiao et al., 2016; Lachlan et al., 2018) but also to improve the drift forecasting (Drivdal et al., 2014).

2.2. 3D oil spill model

The oil spill model developed in this project has two components: (1) a transport model to simulate/project the 3D trajectories of oil particles, and (2) an oil weathering model to simulate oil weathering processes.

a. The transport model

Given that oil from the *Sanchi* leaked continuously at least for 20 days (unreleased report), the crack must be small, with a relatively slow leak rate. Normally, subsurface blowout includes three successive stages: the turbulent jet stage, the buoyant plume stage and the advection-diffusion stage (Socolofsky et al., 2011; Chen et al., 2015). Unlike a violent blowout, which often occurs in oil pipeline ruptures at the sea bottom (Yapa and Zheng, 1997; Zheng and Yapa, 1998; Lardner and Zodiatis, 2017), the oil release from the *Sanchi* is assumed to be relatively slow; thus, we do not include the plume model and only consider the advection-diffusion stage in this study. In the advection-diffusion stage, the spilled oil is divided into a large number of discrete droplets with each particle representing a set of oil droplets. The oil particle is characterised by its spatial coordinates, including velocity and volume. The driving factors for the motion of oil in the water column and at the sea surface are different; thus, the 3D displacement of the spilled oil can be calculated by the following equations.

Eq. (1) is for virtual oil particles in the water column:

$$\frac{d\vec{x}(t)}{dt} = \vec{u}_a\left(\vec{x},t\right) + \vec{u'}\left(\vec{x},t\right) + w\left(\vec{x},t\right)\vec{k} \tag{1}$$

and Eq. (2) is for oil particles at the sea surface:

$$\frac{d\vec{x}(t)}{dt} = \vec{u}_a\left(\vec{x},t\right) + c_w\vec{u}_w\left(\vec{x},t\right) + c_s\vec{u}_s\left(\vec{x},t\right) + \vec{u'}\left(\vec{x},t\right) \tag{2}$$

where $\vec{x}(t)$ denotes the oil position at time t. $\vec{u}_a$, $\vec{u'}$ and w represent the advection, diffusion and buoyancy velocities, respectively. $\vec{u}_w$ and c_w are the wind velocity at a 10 m height over the sea surface and the wind drag coefficient, respectively. $\vec{u}_s$ and c_s are the surface wave–induced Stokes drift and the corresponding wave coefficient, respectively.

The diffusion of oil particles is mainly caused by turbulent mixing, with the diffusion velocity at each time step usually calculated by the random walk technique, as follows:

$$\vec{u'} = R\sqrt{\frac{6\vec{K}}{\Delta t}} \tag{3}$$

where R is a uniformly distributed random number between −1 and 1 and $\vec{K}$ is the diffusion coefficient, which can be obtained from the OFS.

The buoyancy velocity, which is uncorrelated with the setup of the vertical layers, can be evaluated using the equation provided by Zheng and Yapa (2000), which is associated with oil droplet size, oil density and seawater viscosity. Droplet size distribution in subsurface oil spills has been extensively researched, and various calculation approaches have been derived for various situations (Nissanka and Yapa, 2018). Among these approaches, the Rosin-Rammler distribution was widely used and proved to be well fit the laboratory and field experiments (Gonçalves et al., 2016; Johansen et al., 2013).

Wind drift is another important factor in the trajectories of oil particles at the sea surface. Previous studies have shown that the model result is sensitive to the drag coefficient (Abascal et al., 2009), with its value varying from 1.0% to 4.5% (ASCE, 1996; Samuels et al., 1982; Abascal et al., 2009; Zelenke et al., 2012). In this study, by calibrating these values with the SAR images, we found that 2.5% is reasonable. The real-time wind fields used are the same as those in the OFS.

The Stokes drift is the lateral displacement in the direction of the surface wave motion due to non-closed loops from orbital motions. The drift velocity at depth z is calculated as follows: $\sinh^2$

$$u_s = \frac{H^2\omega k\,\cosh(2k(D-z))}{2\,sinh^2(kD)} \tag{4}$$

where H, k, ω and D are the wave amplitude, wave number, wave frequency and water depth, respectively. Each of these parameters is provided by the MASNUM surface wave model.

This model uses a simple beaching algorithm to study the influence of spill oil on the beach. At each time step after the particle been moved, the new oil position was checked to see if it is on shore or in the water. It should be noted that the oil-shore interaction is a very complicated process. The calculations in our study do not include the refloat process for oil washed up on the shore. If the new position is on shore, the oil particle was considered to 'death' and will never be back to water.

b. The oil weathering model

Oil slicks on the sea surface experience oil weathering processes after oil spills. As the *Sanchi* shipwreck involves both condensate and bunker oil leakage, the oil weathering processes we mainly consider are spreading, dissolution, evaporation and emulsification, which are complex and act simultaneously.

2.2.1. Spreading

Oil spill on the sea surface will rapidly thin and broaden, which is recognized as the spreading, due to the counterbalance between driving forces (gravity and surface tension) and retarding forces (inertia and viscosity). This process goes through three phases: gravity-inertia, gravity-viscous, and surface tension-viscous (Fay, 1971), with the first phase occurring quickly and the second phase following closely. Spreading is stopped when the final slick area reaches to $10^5V^{3/4}$ m^2 and the thickness reduces to 10^{-5} $V^{1/4}$m (Fay, 1971), where V is the total volume of the slick.

2.2.2. Dissolution

Dissolution of oil may cause biological harm by increasing the toxicity of the water. The components of oil that easily evaporate are also likely to have a high solubility. Based on algorithms developed by Cohen et al. (1980) and Huang and Monastero (1982), the rate of dissolution for typical oil can be quantified as follows:

$$\frac{dm_{diss}}{dt} = K_d \cdot A_d \cdot S_0 \cdot e^{-0.1t}, \tag{5}$$

where m_{diss} is the mass loss (kg) due to dissolution, K_d is the dissolution mass transfer coefficient (0.01 $m \cdot h^{-1}$), A_d represents the surface area either for oil droplets underwater or oil slicks on the sea surface (m^2), and S_0 is the initial solubility of oil in water, which is related to the oil's properties (usually the API), with a smaller API corresponding to weaker solubility (Lu and Polak, 1973).

2.2.3. Evaporation

Compared with other oil spills, the *Sanchi* disaster is unique in that most of the released oil was condensate, which is light and can evaporate easily. Evaporation begins immediately when the oil rises to the sea surface. The amount and rate of evaporation depend on the percentage of volatile components in the oil. Evaporation is one of the most important physical-chemical processes for reducing the oil volume in this oil spill. Here, we calculate the evaporation rate of the condensate and bunker oil using the formula developed by Mackay et al. (1980), adjusting the evaporation rate of the bunker oil to reflect emulsification (Lehr et al., 1994). The volume fraction of oil evaporation is determined as follows:

$$\frac{dF}{dt} = \frac{K_E}{CK_E t + 1/P_0} \tag{6}$$

$$K_E = K_M^e A v/(RTV_0) \tag{7}$$

where A, v, R, T and V_0 represent the spilled area, molar volume, gas constant (82×10^{-6} atm·m^3/mol·K), surface temperature of the oil and initial spill volume, respectively. Here, A is calculated according to Fay's equation (Fay, 1971). K_M^e is the mass transfer coefficient of evaporation. For bunker oil, $K_M^e$is corrected for emulsification using the following equation (Lehr et al., 1994):

$$K_M^e = K_M(1-E) \tag{8}$$

where $K_M = 0.0025u_w^{0.78}$ is the mass transfer coefficient of the evaporation and E is the instantaneous water content of the emulsion (%). P_0 is the initial vapor pressure in the atmosphere at ambient air temperature T_E:

$$\ln P_0 = 10.6\left(1-\frac{T_0}{T_E}\right) \tag{9}$$

where T_0 is the initial boiling point, which is determined by the oil type. C is a constant and can be determined using the API index (Shen and Yapa, 1988):

$$C = 1158.9API^{-1.1435} \tag{10}$$

2.2.4. Emulsification

Due to wave breaking and sea surface turbulence, spilled oil, particularly crude and residual oils, mixes with the water column to form emulsions (Shen and Yapa, 1988). Emulsification can increase the oil's volume, density and viscosity and retard evaporation. Here, the emulsification process is only considered for bunker oil due to the rapid evaporation rate of condensate oil. Emulsification is usually estimated by the water content of the oil, which can be calculated using the following formula proposed by Mackay et al. (1980):

$$\frac{dE}{dt} = k\left(1+\vec{u}_w\right)^2\left(1-\frac{E}{E_f}\right) \tag{11}$$

where E and E_f are the instantaneous and final water content of the emulsion (%), respectively. k is the mass transfer coefficient of emulsification, with a value usually ranging from 1.0×10^{-6} to 2.0×10^{-6}; here, we take the default value of 1.6×10^{-6} from the MOHID and ADIOS models (NOAA, 1994).

The values of all the parameters discussed here are listed in Tables 1 and 2.

2.3. Design of the numerical experiments

3D historical and real-time forecasting, in addition to forcing hydrometeorological data (temperature, ocean currents, wind and surface waves) from the OFS with a time step of 3 h, was used to simulate and project the fate of the oil spilled from the *Sanchi*. Virtual oil particles were tracked hourly by using OFS outputs linearly interpolated to 1 h. We first calibrated the wind drift factor by comparison with SAR images and validated it using observational reports based on real-time data from the 2 months after the *Sanchi* sank. Next, four numerical experiments were implemented to explore the pollution probability under various scenarios according to the oil properties and various emission periods. The latter four experiments were based on historical OFS data from 14 January to 14 July for the years from 2009 to 2017. The configuration of all six runs is shown in Table 3. Unlike the traditional oil spill model simulations, our focus in this study is to give a map of pollution probability in certain areas based on statistical analysis, rather than pollution severity. As the oil from the *Sanchi* leaked continuously for at least 20 days (unreleased report), our release periods were set at 60 days and 180 days to obtain the different maximum pollution maps.

The pollution probability in a certain time period was estimated by 'visitation frequency' (Csanady, 1983; Chang et al., 2011). The whole domain that we simulated was divided into bins with a resolution of 0.1° by 0.1° (10.7–7.4 km for the latitudes 15°–48°N). The 'visitation frequency' of each bin, which is a proportion, was calculated by dividing the accumulated amount of oil particles that reached each bin by the total amount of particles emitted from the *Sanchi* over 60 days or 180 days (Table 3). This reflects the probability of the emitted particles from the shipwreck location reaching a certain bin during a certain time period.

To check whether OFS output with a time step of 3 h can simulate the trajectories of oil slicks correctly, we run comparison experiments with the OFS output of 3 h, 1 h and 0.5 h, respectively. Difference exists in trajectories for single particle for different time steps one month after the *Sanchi* sank. However, from a statistical point of view, the spatial distributions of particle trajectories and potentially contaminated areas from simulations with higher time resolutions (1 h and 0.5 h) and relatively low resolution (3 h) are consistent (Figs. S1 and S2).

Table 1
Environmental parameters for the oil spill model.

Parameter	Value
Sea water viscosity ν_w (N s/m^2)	10^{-6} (Chen et al., 2015)
Location of the *Sanchi* wreckage	28°22′N, 125°55′E, 115 m underwater
Wind speed (m/s)	From the OFS
Sea surface temperature (K)	From the OFS
Air temperature (K)	The same as the sea surface temperature

Table 2
Oil properties and parameters for the oil spill model.

Parameters	Oil type	
	Condensate	Bunker
Oil viscosity ν (m^2/s)	$0.6958 \times 10^{-6*}$	1.88×10^{-5} (Shen and Yapa, 1988)
Density (20 °C, g/cm^3)	0.7424*	0.9672 (calculated based on Shen and Yapa, 1988)
Initial boiling point T_0 (K)	311.15*	338.4 (calculated based on Shen and Yapa, 1988)
API index	58*	14.8 (Lu and Polak, 1973)
Molar volume (m^3/mol)	600×10^{-6} (Shen and Yapa, 1988)	200×10^{-6} (Shen and Yapa, 1988)
Initial solubility of oil in water (kg/m^3)	0.0884 (Lu and Polak, 1973)	0.00104 (Lu and Polak, 1973)
Dissolution decay constant α (h^{-1})	0.1 (Lu and Polak, 1973)	0.017 (Lu and Polak, 1973)

Note: the symbol * indicates that the value was based on experimental records from the State Oceanic Administration, China.

3. Results and discussion

3.1. Oil spill model calibration

To calibrate the wind drag coefficient used in the oil spill model, the oil particle trajectories simulated based on real-time data up to 1 April 2018 were compared with the oil slicks observable from CosmoSkyMed SAR images (Simulation 1 from Table 3). The short-term simulation illustrates the spatiotemporal distribution of the oil particles, which represents potentially polluted locations. The blue and yellow dots in Fig. 1 indicate the simulated distributions of oil particles for condensate and bunker oil, respectively, and the corresponding oil slicks observable in SAR images are encircled in white. Fig. 1 shows that the simulated distribution of the oil particles is generally consistent with the oil slicks in the synchronous SAR images, although discrepancies exist. The discrepancies are likely due to uncertainties in the leakage information, such as the remaining oil amount, leakage rate, crack diameter, geometry and other parameters used in the oil spill model, as well as the reasonable mismatch may also from the surface wav-tide-circulation coupled model (Tables 1 and 2). Because the root mean square error increases linearly with the simulation time (De Dominicis et al., 2013a, 2013b), discrepancies exist for long-term simulations. The largest discrepancy between the simulation results and SAR images is approximately 11 km, on day 7 of the simulation (i.e., the seventh day after the *Sanchi* sank) (Fig. 1d), which falls within the acceptable level of variance between model simulations and observations (De Dominicis et al., 2013b; Cheng et al., 2011).

After calibration using synchronous SAR images, the simulated results (Simulation 2 from Table 3) were also compared with synchronous observations from 14 January to 1 April 2018, as shown in Fig. 2. The colours of the dots and circles in Fig. 2a indicate the days after the *Sanchi* sank. If the days of the observations (circles) are later than or consistent with the simulations (dots), the simulation results are consistent with the observations. In general, the beaching time and locations of oil particles from the model simulation are consistent with the actual appearance of oil spill on shore, with discrepancies increasing with the simulation time (Fig. 2b). Both the simulated results and observational reports (JCG, 2018) indicate that oil slicks from the *Sanchi* could reach the Ryukyu Island Chain, which is south and west of the shipwreck location.

Although the regions south and west of the shipwreck on the edge of the Ryukyu Island Chain are the areas with the highest likelihood of pollution by the *Sanchi* oil spill, the trajectories of oil particles show a tendency to expand along two routes: (1) the East China Sea, with some virtual oil particles entering the Sea of Japan, and (2) the North Pacific Ocean, along the strong Kuroshio Current. Although information on the fate of the spill and the oil properties remains limited, the simulation results in this study are consistent with the space-borne SAR and observational reports.

3.2. Potentially contaminated areas at the sea surface

After validation by comparison with SAR images and reported oil pollution areas, we ran the model with four scenarios by considering oil properties and varying emission periods to produce a map of potentially contaminated areas at the sea surface. Table 3 shows the model simulation information. Simulation 3 was performed to simulate the distribution of oil particles only from the condensate. Simulations 4 and 5 were performed using the same settings as in Simulation 3 but including bunker oil leakage; we used different emission periods for the bunker oil in each simulation to investigate its impact on the results.

The droplet size distribution (DSD) influences the vertical velocity of spill oil, and subsequently the volume fraction of dissolved oil in the water column, as well as the surface horizontal distribution of the spill oil. However, there exists high uncertainty of the DSD. To test the range of underwater dissolution rate and the influence of DSD on the oil horizontal distribution, we use the Rosin-Rammler distribution with the range of the fiftieth percentile (d_{50}) between 200 μm and 900 μm following Gonçalves's definition (Gonçalves et al., 2016). Results show that most of the oil droplets leaking from the *Sanchi* wreck (115 m underwater) float to the surface within 1 to 4 h for condensate and 1.5 to 13 h for bunker oil (Figure not shown here). Approximately 0.5%~5.4% of the total condensate and 0–0.1% of the bunker oil dissolve in the water during passage from the spill location to the sea surface. Range of the dissolution rate based on the above droplet size distribution at each depth layer for the two types of oil is shown in Fig. S4 (a) in the supplementary information. The test also imply that in these size ranges, the short residence time of spill oil at the subsurface will have only a minor effect on the long-term (up to 180 days) statistical results.

Table 3
Design of the numerical runs performed in this study.

No. of simulations	Releasing depth	Dimension	Oil type	Tracking time	Releasing duration	Releasing frequency (particles/h)	Current database
1	115 m	3D	Condensate + bunker	16 days	60 days	500:500	Real-time
2	115 m	3D	Bunker	60 days	60 days	1000	Real-time
3	115 m	3D	Condensate	180 days	180 days	1000	2009–2017
4	115 m	3D	Bunker	180 days	60 days	1000	2009–2017
5	115 m	3D	Bunker	180 days	180 days	1000	2009–2017
6	10 m	2D	Condensate + bunker in water column	180 days	180 days	500:500	2009–2017

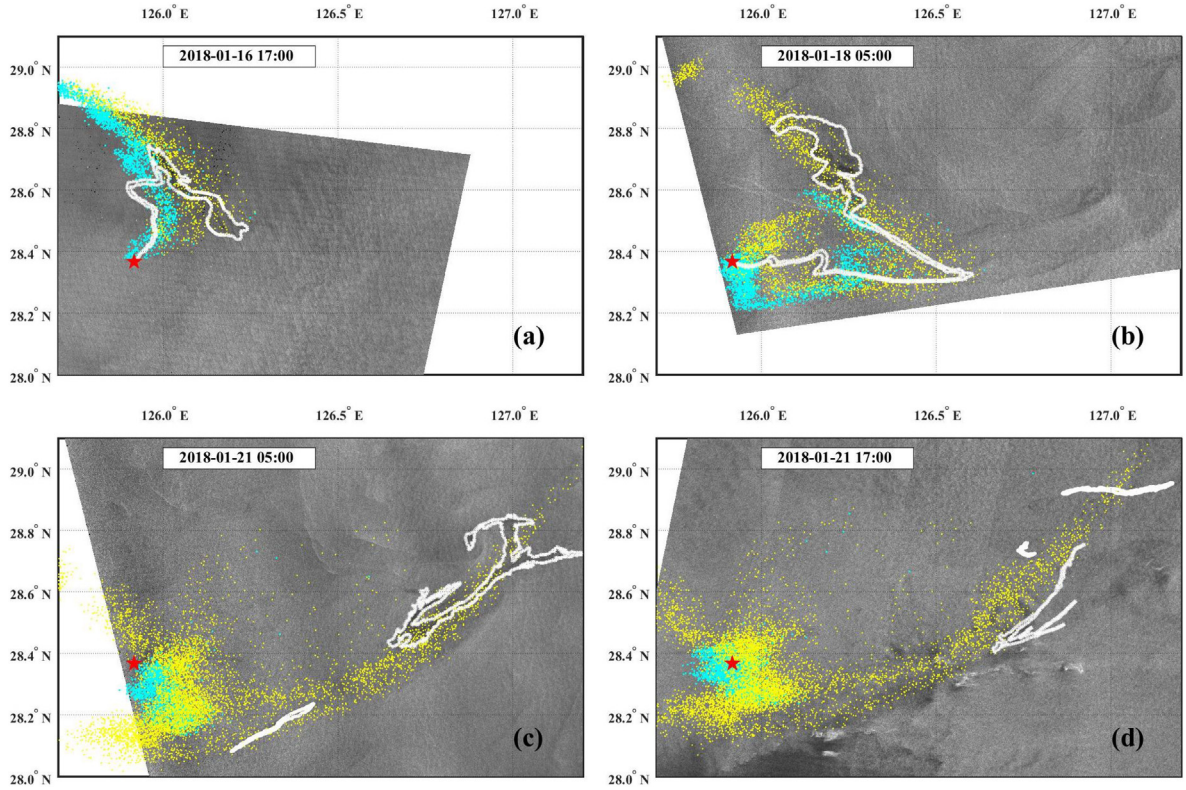

Fig. 1. Simulated trajectories of the condensate (blue) and bunker (yellow) oil particles leaked from the *Sanchi* (red star) at (a) 17:00 on 16 January 2018, (b) 05:00 on 18 January 2018, (c) 05:00 on 21 January 2018, and (d) 17:00 on 21 January 2018. The underlying grey images are the Cosmo-SkyMed ScanSAR images. The oil stripes shown on the SAR images are encircled in white.

Because oil begins to evaporate immediately after it reaches the sea surface, most of the condensate volume is lost via evaporation within days (Fig. S4(b)). In contrast, the bunker oil emulsifies and eventually forms a mousse within one day (Fig. S4(c)), which means that the evaporation is retarded and the emulsified oil persists on the sea surface for a longer time if it is not washed up on shore. The model results show that approximately 20% of the bunker oil evaporates within 48 h (Fig. S4(b)) and the proportion increases to 30% over 180 days of the shipwreck, with the residual 70% floating after a long time floating on the sea surface in the form of tar lumps or below the sea surface in the form of tiny droplets, or washed on shore.

Simulation 3: Potentially contaminated areas at the sea surface due to condensate alone.

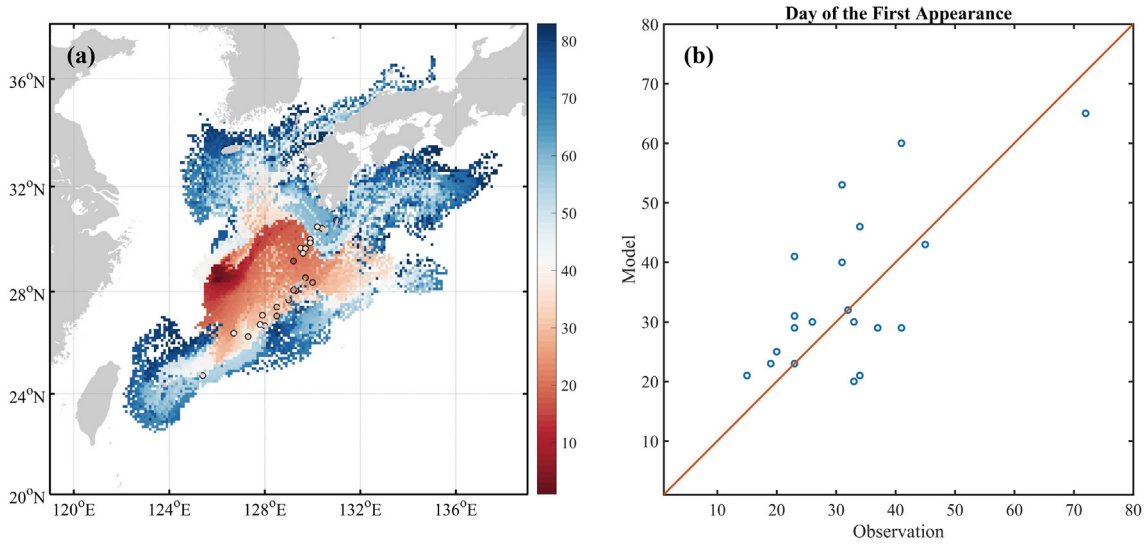

Fig. 2. Comparison between simulated virtual oil particles (coloured dots) and reported oil pollution sites (coloured circles, JCG, 2018) up to 1 April 2018 (a), and comparison between the day of first appearance on shore in the model simulation and observation (b). In panel (a), the colour indicates the number of days after the *Sanchi* sank. Dots and circles of various colours indicate the days after the *Sanchi* sank. If the days in the observation (circles) are later than or consistent with the simulation (dots), the simulation results are consistent with the observations.

Despite the rapid evaporation rate of the condensate oil, a statistical account of the pollution probability is still needed due to the large amount of condensate oil that sank with the *Sanchi*. In this numerical experiment, the weathering process of condensate oil spilled from 14 January to 14 July 14 for the years 2009 to 2017 is examined, and the horizontal effect range of the oil is derived from the coupled model. It should be noted that although condensate oil particles may emulsify, they are relatively unstable (Sebastião and Guedes Soares, 1995). Therefore, when we track oil slicks from the condensate alone, the main processes to consider are dissolution and evaporation. The initial oil thickness calculated according to Fay's equation ranges from 25 to 40 μm for release durations of 180 days and 30 days, respectively. Previous simulations have used 0.1 mm for crude oils and a smaller number for light refined products (Reed, 1989; Lehr, 2001); here, we chose the maximum initial oil thickness (0.1 mm) for both types of oils to obtain the maximum potential pollution region with the aim to give a 'minimum regret' estimation. This value also falls in the range of observational values (data reports not shown). Statistical analysis shows that the evaporation time for most condensate oil slick is no more than 2 days. The entire condensate on the sea surface will evaporate within 4 days (Fig. S4(b) in the supplementary information). Fig. 3 shows the map of the potential extent of the oil spill at the sea surface only for condensate over different time periods. Because the condensate evaporates easily, potentially polluted regions with continuous leakage up to 180 days are restricted to a 100 × 100-km area around the shipwreck location. From a detailed analysis of the relationship between the wind and the regions affected by condensate in each month, we found that the drifting of condensate oil slicks is dependent on the wind and ocean currents. It can be clearly observed that the potential extent of the condensate oil spill is mainly located northeast of the shipwreck as a result of the ocean current; however, from January to March, the oil slicks tended to move to the southeast of the shipwreck due to strong northwest winds (the highest wind speed was more than 18 m/s).

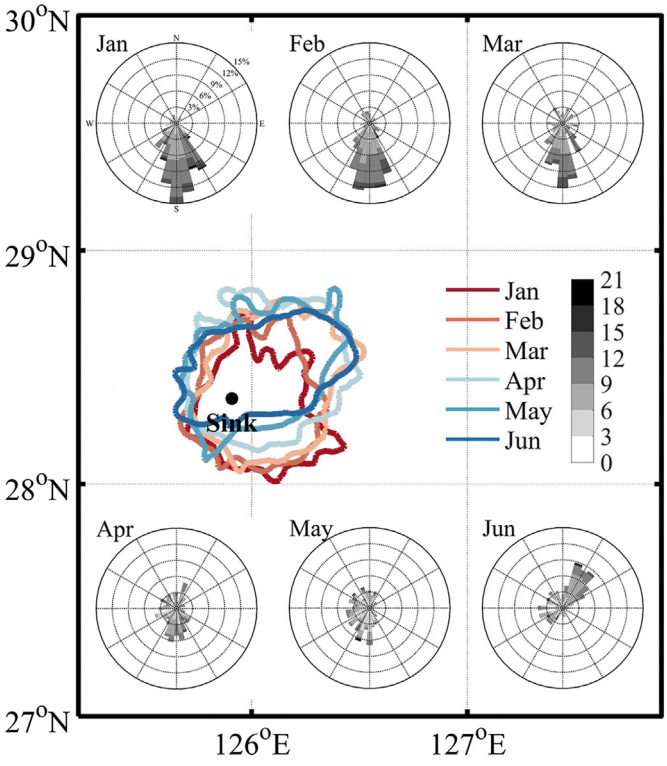

Fig. 3. Potentially contaminated areas due to the condensate oil spill for different time periods. The corresponding wind rose maps are presented from January to June.

Simulations 4 and 5: Potentially contaminated areas at the sea surface due to bunker oil.

Heavy oil types such as bunker oil are easily emulsified on the sea surface to form a viscous mousse, which will persist in the ocean for a long period. In particular, rough sea conditions in the winter are favourable for the formation of mousse, which then decomposes into tar lumps (Kingston, 2002). Two simulations of tar lumps were run to estimate the pollution probability of surrounding areas in various emission scenarios.

Fig. 4 and Fig. S3 show the maps of the potential extent of the oil spill and the 'visitation frequency' of oil pollutants reaching a particular part of the ocean, based on the assumption that the bunker oil leaks for 2 months and 6 months, respectively. It is estimated that 30% to 50% of the oil was trapped on the shore, with the highest pollution probability in the two scenarios being given for the Ryukyu Island Chain, Tsushima Strait, on the south and east coast of Japan. This result is consistent with the observational report from the Japan Coast Guard (JCG, 2018). The proportions of oil particles that wash up on the shore in Simulation 4 are 26%, 44%, 46% and 49%, for 60, 90, 120 and 180 days after the sinking of the *Sanchi*, respectively. In Simulation 5, in which the oil is released continuously, the beaching proportions in various periods remain basically consistent at approximately 30%. Thus a large amount of oil could be trapped by oil-shore interactions and affect the coastal environment. It should be noted that the oil-shore interaction is a very complicated process. The calculations in our study do not include the re-float process for oil washed up on the shore, thus the beaching amount may be overestimated.

In addition, potentially polluted ocean areas at the sea surface expand to most of the region southeast of the *Sanchi* wreck (17–43°N, 120–155°E), with the northernmost and southernmost areas lying the North Pacific Ocean east of Hokkaido Island and the Luzon Strait, respectively. The wind effect is likely responsible for the northernmost potentially contaminated areas, located in the north of the Kurohio Extension. Although no large differences are seen between the two simulations, a comparison of Fig. 4e with Fig. S3e shows that the Yellow Sea could be affected by a long release period due to the seasonal change of the wind direction and ocean currents.

Unlike the NOC simulations, which treat the vicinity of Amami Ōshima Island as the release site (NOC, 2018b), the oil particles in our simulations are released from the final site of the *Sanchi* shipwreck. Although the general pattern of the potentially contaminated areas is consistent between the two models, a small risk of contamination remains in the Yellow Sea according to our statistical analysis (Fig. S3).

3.3. Potentially contaminated areas due to subsurface oil-contaminated water

When oil leaked from the *Sanchi* wreck, the dissolved components from the oil particles and tiny droplets that remained underwater, as well as those dispersed into the water column as a result of surface waves and turbulence, were subject to subsurface transport. Simulation 6 presents the area potentially contaminated due to subsurface oil-contaminated water (Fig. 5). Compared with surface oil particles, subsurface (10 m below the surface) oil-contaminated water mainly travels along the ocean currents and expands along two routes: (1) entering the Sea of Japan through the Tsushima Strait, where the contamination persists, and (2) expanding to the south coast of Japan and the North Pacific Ocean along the strong Kuroshio Current. Without the wind effect, most particles are found north of the *Sanchi* wreck along the Tsushima Current. Compared with our previous study, which found that the regions along the Kuroshio were mainly affected (Yin et al., 2018), our refined simulations using a 3D oil spill model based on statistical analysis show the Sea of Japan to be the other area most likely to be polluted by subsurface oil-contaminated water.

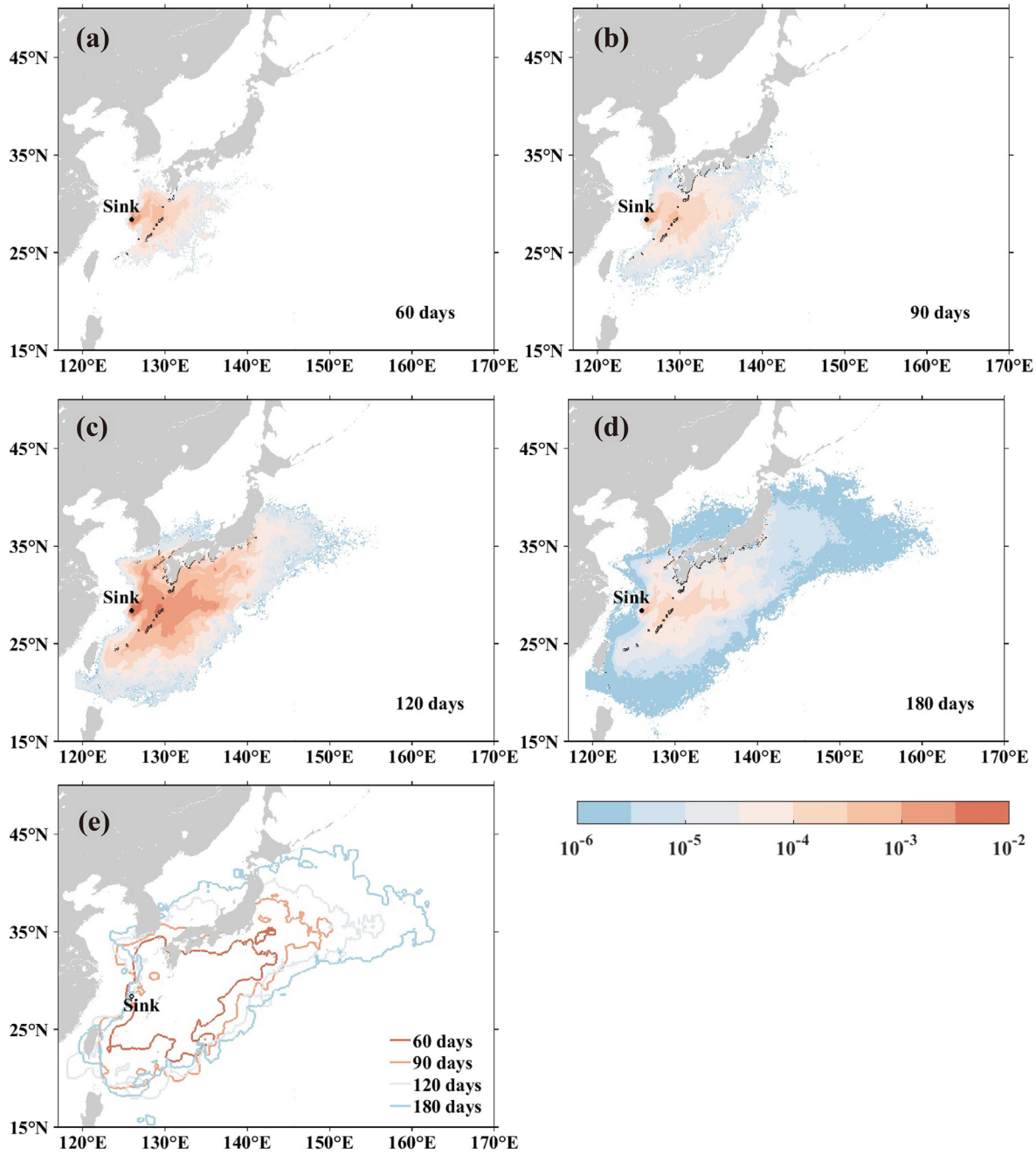

Fig. 4. Maps of the visitation frequency for oil particles (a–d) and potentially contaminated areas for various time periods (e), based on the assumption that the bunker oil leaks continuously for 2 months. The coastal areas affected (beaching) are marked in black (a–d).

3.4. Uncertainty discussion

It should be noted that the model is sensitive to various factors, such as errors in the initial input data, details of the release, the wind/ocean current, time step etc. (Simecek-Beatty, 2011), and other weathering process such as biodegradation. Because the crack diameter, geometry and the location are unknown, uncertainties still exist concerning the leakage rate and the initial emission setup. Due to the sophisticated situation of the *Sanchi* oil spill event (two types of oils leaked from the ship wreckage) with limited in-situ information, we simplify the releasing details based on available observational reports, and give a statistically analysis for potential polluted areas at different spilling scenarios. For a further research to better convey the uncertainty, the ensemble forecasting with a compilation of output from different initial conditions and models can be used (Simecek-Beatty, 2011). Further surveys and research should be performed to explore these topics.

4. Conclusions

We established a comprehensive 3D oil spill model to simulate and estimate pollution probabilities based on leakage from the *Sanchi* wreckage. Wind, ocean current and surface wave data produced by the OFS were used to track oil particles up to 180 days after the *Sanchi* sank. Short-term simulations show patterns consistent with the synchronous SAR images and observations. The potentially contaminated areas depend on the properties of the released oil.

Three different scenarios, in which oil particles are released either from the condensate or the bunker oil from the *Sanchi* shipwreck,

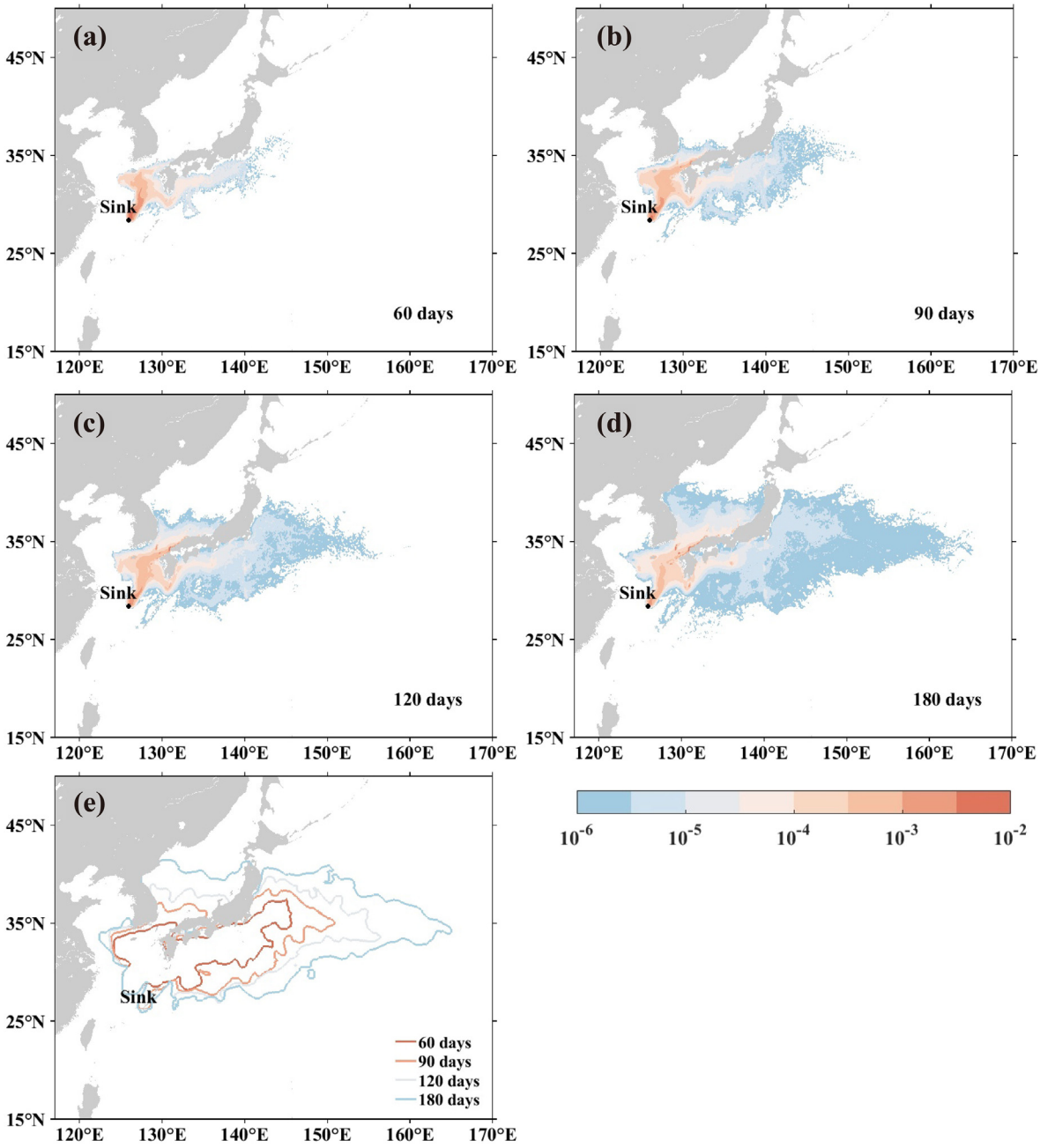

Fig. 5. Cumulative trajectories of the subsurface oil-contaminated water (a) 60 days, (b) 90 days, (c) 120 days and (d) 180 days after the *Sanchi* sank, and (e) potentially contaminated areas due to the subsurface oil-contaminated water for various time periods. The affected coastal areas are marked in black.

were evaluated to give a probability map of potentially polluted areas. Due to the fast evaporation, the distribution of the surface condensate oil slicks was confined to regions within a 100 × 100-km area around the location of the shipwreck because of the rapid evaporation rate, with the contaminated regions being closely associated with wind effects. For the leaked bunker oil, the highest pollution probability was mainly in the Ryukyu Island Chain and southeast of the *Sanchi* wreck, and also in the North Pacific due to the effects of a northerly wind and surface wave Stokes drift. Moreover, the Yellow Sea could be potentially affected over a long release period, mainly due to the change in wind direction and currents. It was estimated that 30% to 50% of the oil was trapped on the shore, with the highest pollution probability in the two scenarios occurring in the Ryukyu Island Chain, Tsushima Strait, on the south and east coasts of Japan. In addition, subsurface oil-contaminated water was likely to enter the Sea of Japan along Tsushima Strait and the south coast of Japan, in addition to the North Pacific Ocean along the strong Kuroshio Current. These results are essential for tracking the leaked oil and performing pollution assessments.

Declaration of Competing Interest

The authors declare no conflict of interest.

Acknowledgments

The outputs from the OFS are freely available from a long-term archive FTP website (http://data.fio.org.cn/qiaofl/OSP). All authors are jointly supported by the international cooperation project on the China-Australia Research Center for Maritime Engineering of Ministry of Science and Technology, P. R. China (2016YFE0101400), the National Natural Science Foundation of China (NSFC)-Shandong Joint Fund for Marine Science Research Centers (U1606405), the international

cooperation project on Indo-Pacific ocean environmental variability and air-sea interactions (GASI-IPOVAI-05), and the Aoshan Talents Cultivation Excellent Scholar Program supported by Qingdao National Laboratory for Marine Science and Technology (2017ASTCP-ES04).

Appendix A. Supplementary data

Supplementary data to this article can be found online at https://doi.org/10.1016/j.scitotenv.2019.06.255.

References

Aali, J., Rahmani, O., 2012. H_2S—Origin in South Pars gas field from Persian Gulf. Iran. J. Pet. Sci. Eng. 86-87, 217–224. https://doi.org/10.1016/j.petrol.2012.03.009.

Abascal, A.J., Castanedo, S., Mendez, F.J., Medina, R., Losada, I.J., 2009. Calibration of a Lagrangian transport model using drifting buoys deployed during the 'Prestige' oil spill. J. Coast. Res. 25 (1), 80–90. https://doi.org/10.2112/07-0849.1.

Alonso-Alvarez, C., Pérez, C., Velando, A., 2007. Effects of acute exposure to heavy fuel oil from the Prestige spill on a seabird. Aquat. Toxicol. 84 (1), 103–110. https://doi.org/10.1016/j.aquatox.2007.06.004.

ASA, 1997. OILMAP for Windows. ASA Inc, Rhode Island (Ed.).

ASCE, 1996. State-of-the-art review of modeling transport and fate of oil spills. J. Hydrol. Eng. 122 (11), 594–609. https://doi.org/10.1061/(ASCE)0733-9429.

Berry, A., Dabrowski, T., Lyons, K., 2012. The oil spill model OILTRANS and its application to the Celtic Sea. Mar. Pollut. Bull. 64 (11), 2489–2501. https://doi.org/10.1016/j.marpolbul.2012.07.036.

Carracedo, P., Torres-López, S., Barreiro, M., Montero, P., Balseiro, C.F., Penabad, E., Leitao, P.C., Pérez-Muñuzuri, V., 2006. Improvement of pollutant drift forecast system applied to the Prestige oil spills in Galicia Coast (NW of Spain): development of an operational system. Mar. Pollut. Bull. 53 (5), 350–360. https://doi.org/10.1016/j.marpolbul.2005.11.014.

Carswell, C., 2018. Unique oil spill in East China Sea frustrates scientists. Nature 554, 17–18. https://doi.org/10.1038/d41586-018-00976-9.

Cekirge, H.M., Koch, M., Long, C., Giammona, C.P., Binkley, K., Engelhardt, R., Jamail, R., 1995. State-of-the-art techniques in oil spill modeling. Int. Oil Spill Conf. Proc. 1995 (1), 67–72. https://doi.org/10.7901/2169-3358-1995-1-67.

Chang, Y.L., Oey, L., Xu, F.H., Lu, H.F., Fujisaki, A., 2011. 2010 oil spill: trajectory projections based on ensemble drifter analyses. Ocean Dyn. 61 (6), 829–839. https://doi.org/10.1007/s10236-011-0397-4.

Chen, H., Wei, A., You, Y., Lei, F., Zhao, Y., Li, J., 2015. Numerical study of underwater fate of oil spilled from deepwater blowout. Ocean Eng. 110, 227–243. https://doi.org/10.1016/j.oceaneng.2015.10.025.

Cheng, Y., Li, X., Xu, Q., et al., 2011. SAR observation and model tracking of an oil spill event in coastal waters. Mar. Pollut. Bull. 62 (2), 350–363.

Cohen, Y., Mackay, D., Shiu, W.Y., 1980. Mass transfer rates between oil slicks and water. Can. J. Chem. Eng. 58 (5), 569–575. https://doi.org/10.1002/cjce.5450580504.

Cox, C.S., Zhang, X., Duda, T.F., 2017. Suppressing breakers with polar oil films: using an epic sea rescue to model wave energy budgets. Geophys. Res. Lett. 44 (3), 1414–1421. https://doi.org/10.1002/2016GL071505.

Csanady, G.T., 1983. Dispersal by randomly varying currents. J. Fluid Mech. 132, 375–394. https://doi.org/10.1017/S0022112083001664.

De Dominicis, M., Pinardi, N., Zodiatis, G., Lardner, R., 2013a. MEDSLIK-II, a Lagrangian marine surface oil spill model for short-term forecasting—part 1: theory. Geosci. Model Dev. 6, 1851–1869. https://doi.org/10.5194/gmd-6-1851-2013.

De Dominicis, M., Pinardi, N., Zodiatis, G., Archetti, R., 2013b. MEDSLIK-II, a Lagrangian marine surface oil spill model for short-term forecasting—part 2: numerical simulations and validations. Geosci. Model Dev. 6, 1871–1888. https://doi.org/10.5194/gmd-6-1871-2013.

Delgado, L., Kumzerova, E., Martynov, M., 2006. Simulation of oil spill behaviour and response operations in PISCES. WIT Trans. Ecol. Environ. 88, 279–292. https://doi.org/10.2495/CENV060271.

Drivdal, M., Broström, G., Christensen, K.H., 2014. Wave induced mixing and transport of buoyant particles: application to the Statfjord A oil spill. Ocean Sci. 10 (3), 977–991. https://doi.org/10.5194/os-10-977-2014.

Fay, J.A., 1971. Physical processes in the spread of oil on a water surface. Proc. Joint Conf. Prev. Control Oil Spills 463–467.

Gonçalves, R.C., Iskandarani, M., Srinivasan, A., Thacker, W.C., Chassignet, E., Knio, O.M., 2016. A framework to quantify uncertainty in simulations of oil transport in the ocean. J. Geophys. Res. Oceans 121 (4), 2058–2077.

Guo, X., Miyazawa, Y., Yamagata, T., 2006. The Kuroshio onshore intrusion along the shelf break of the East China Sea: the origin of the Tsushima warm current. J. Phys. Oceanogr. 36 (12), 2205–2231. https://doi.org/10.1175/JPO2976.1.

Huang, J.C., Monastero, F.C., 1982. Review of the State-of-the-Art of Oil Spill Simulation Models. Final Report Submitted to the American Petroleum Institute. Raytheon Ocean Systems Company, East Providence, RI.

Japan Coast Guard (JCG), 2018. Report for Oil Contamination from Sanchi. retrieved 16 August 2018 from. http://www.kaiho.mlit.go.jp/info/images/yujoubutu.pdf.

Johansen, Ø., Brandvik, P.J., Farooq, U., 2013. Droplet breakup in subsea oil releases-part 2: predictions of droplet size distributions with and without injection of chemical dispersants. Mar. Pollut. Bull. 73 (1), 327–335. https://doi.org/10.1016/j.marpolbul.2013.04.012.

Kingston, P.F., 2002. Long-term environmental impact of oil spills. Spill Sci. Technol. Bull. 7 (1), 53–61. https://doi.org/10.1016/S1353-2561(02)00051-8.

Lachlan, S., Walsh, K.J.E., Thomas, S., Spence, P., Babanin, A.V., 2018. Changes in ocean heat content caused by wave-induced mixing in a high-resolution ocean model. J. Phys. Oceanogr. 48 (5), 1139–1150. https://doi.org/10.1175/jpo-d-1117-0142.1171.

Lardner, R., Zodiatis, G., 2017. Modelling oil plumes from subsurface spills. Mar. Pollut. Bull. 124, 94–101.

Lee, R.F., Dornseif, B., Gonsoulin, F., Tenore, K., Hanson, R., 1981. Fate and effects of a heavy fuel oil spill on a Georgia salt marsh. Mar. Environ. Res. 5 (2), 125–143. https://doi.org/10.1016/0141-1136(81)90028-3.

Lee, H.-C., Rosati, A., Spelman, M.J., 2006. Barotropic tidal mixing effects in a coupled climate model: oceanic conditions in the Northern Atlantic. Ocean Model 11 (3), 464–477. https://doi.org/10.1016/j.ocemod.2005.03.003.

Lehr, W.J., 2001. Review of modeling procedures for oil spill weathering behavior. Adv. Ecol. Sci. 9, 51–90.

Lehr, W., et al., 1994. Model sensitivity analysis in environmental emergency management: a case study in oil spill modeling. Proceedings of the 26th Conference on Winter Simulation. Society for Computer Simulation International, Orlando, Florida, USA, pp. 1198–1205.

Lockwood, D., 2018. Sunken oil tanker threatens marine life. Chem. Eng. News 96 (4), 4. https://doi.org/10.1021/cen-09604-notw1.

Lonin, S.A., 1999. Lagrangian model for oil spill diffusion at sea. Spill Sci. Technol. Bull. 5 (5), 331–336. https://doi.org/10.1016/S1353-2561(99)00078-X.

Lu, C.Y., Polak, J., 1973. A study of solubility of oil in water. Report EPS-4-EC-76-1. Environmental Protection Service, Canada.

Mackay, D., Paterson, S., Nadeau, S., 1980. Calculation of the evaporation rate of volatile liquids. Proceedings, National Conference on Control of Hazardous Material Spills, Louisville, Ky, pp. 364–368.

Madec, G., 2012. NEMO Ocean Engine. Institut Pierre-Simon Laplace (IPSL), France (ISSN No 1288-1619).

National Oceanography Center (NOC), Southampton, UK, 2018a. Sanchi oil spill contamination could reach Japan within a month (update). Retrieved 16 January 2018 from. http://noc.ac.uk/news/Sanchi-oil-spill-contaimination-could-reach-Japan-within-a-month-update.

National Oceanography Center (NOC), Southampton, UK, 2018b. Coral reefs may be at risk from Sanchi oil tanker contamination. Retrieved 6 February 2018 from. http://noc.ac.uk/news/coral-reefs-may-be-risk-sanchi-oil-tanker-contamination.

Nissanka, I.D., Yapa, P.D., 2018. Calculation of oil droplet size distribution in ocean oil spills: a review. Mar. Pollut. Bull. 135, 723–734. https://doi.org/10.1016/j.marpolbul.2018.07.048.

NOAA, 1994. NOAA (1994)—ADIOSTM (Automated Data Inquiry for Oil Spills) User's Manual. Hazardous Materials Response and Assessment Division, NOAA. Prepared for the U.S. Coast Guard Research and Development Center, Groton Connecticut, Seattle (50 pp).

Peterson, C.H., Rice, S.D., Short, J.W., Esler, D., Bodkin, J.L., Ballachey, B.E., Irons, D.B., 2003. Long-term ecosystem response to the Exxon Valdez oil spill. Science 302 (5653), 2082–2086. https://doi.org/10.1126/science.1084282.

Qiao, F., Yuan, Y., Yang, Y., Zheng, Q., Xia, C., Ma, J., 2004. Wave-induced mixing in the upper ocean: distribution and application to a global ocean circulation model. Geophys. Res. Lett. 31 (11), 293–317. https://doi.org/10.1029/2004GL019824.

Qiao, F.L., Wang, G.S., Lü, X.G., Dai, D.J., 2011a. Drift characteristics of green macroalgae in the Yellow Sea in 2008 and 2010. Environ. Res. Lett. 56 (21), 2236–2242. https://doi.org/10.1007/s11434-011-4551-7.

Qiao, F., Wang, G., Zhao, W., Zhao, J., Dai, D., 2011b. Predicting the spread of nuclear radiation from the damaged Fukushima Nuclear Power Plant. Environ. Res. Lett. 56 (18), 1890–1896. https://doi.org/10.1007/s11434-011-4513-0.

Qiao, F., Yuan, Y., Deng, J., Dai, D., Song, Z., 2016. Wave–turbulence interaction-induced vertical mixing and its effects in ocean and climate models. Philos. Trans. R. Soc. Lond. A 374 (2065), 1–20. https://doi.org/10.1098/rsta.2015.0201.

Reed, M., 1989. The physical fates component of the natural resource damage assessment model system. Oil Chem. Pollut. 5 (2–3), 51–90. https://doi.org/10.1016/S0269-8579(89)80009-7.

Samuels, W.B., Huang, N.E., Amstutz, D.E., 1982. An oil spill trajectory analysis model with a variable wind deflection angle. Ocean Eng. 9 (4), 347–360. https://doi.org/10.1016/0029-8018(82)90028-2.

Schwartzberg, H.G., 1971. The movement of oil spills. Int. Oil Spill Conf. Proc., 489–494 https://doi.org/10.7901/2169-3358-1971-1-489.

Sebastião, P., Guedes Soares, C., 1995. Modeling the fate of oil spills at sea. Spill Sci. Technol. Bull. 2 (2), 121–131. https://doi.org/10.1016/S1353-2561(96)00009-6.

Shen, H.T., Yapa, P.D., 1988. Oil slick transport in rivers. J. Hydraul. Eng. 114 (5), 529–543 (doi:10.1061/(ASCE)0733-9429).

Simecek-Beatty, D., 2011. Chapter 11-oil spill trajectory forecasting uncertainty and emergency response. In: Fingas, M. (Ed.), Oil Spill Science and Technology. Gulf Professional Publishing, Boston, pp. 275–299.

Socolofsky, S.A., Adams, E.E., Sherwood, C.R., 2011. Formation dynamics of subsurface hydrocarbon intrusions following the Deepwater Horizon blowout. Geophys. Res. Lett. 38 (9), 159–164. https://doi.org/10.1029/2011GL047174.

Sun, S.J., Lu, Y.C., Liu, Y.X., Wang, M.Q., Hu, C.M., 2018. Tracking an oil tanker collision and spilled oils in the East China Sea using multisensor day and night satellite imagery. Geophys. Res. Lett. 45, 3210–3212. https://doi.org/10.1002/2018GL077433.

Toz, A.C., Koseoglu, B., 2018. Trajectory prediction of oil spill with Pisces 2 around Bay of Izmir, Turkey. Mar. Pollut. Bull. 126, 215–227. https://doi.org/10.1016/j.marpolbul.2017.08.062.

Wang, G., Zhao, C., Jiang, L., Qiao, F., Xia, C., 2016. Verification of an operational ocean circulation-surface wave coupled forecasting system for the China's seas. Acta Oceanol. Sin. 35 (2), 19–28. https://doi.org/10.1007/s13131-016-0810-4.

Yang, Y., Qiao, F., Zhao, W., Teng, Y., Yuan, Y., 2005. MASNUM ocean wave numerical model in spherical coordinates and its application. Acta Oceanol. Sin. 27 (2), 1–7.
Yapa, P.D., Zheng, L., 1997. Simulation of oil spills from underwater accidents I: model development. J. Hydraul. Res. 35, 673–687.
Yin, X., Qiao, F., Yang, Y., Xia, C., 2010. An ensemble adjustment Kalman filter study for Argo data. Int. J. Oceanol. Limnol. 28 (3), 626–635. https://doi.org/10.1007/s00343-010-9017-2.
Yin, L., Zhang, M., Zhang, Y., Qiao, F., 2018. The long-term prediction of the oil-contaminated water from the Sanchi collision in the East China Sea. Acta Oceanol. Sin. 3, 1–4. https://doi.org/10.1007/s13131-018-1193-5.
Yuan, Y., Hua, F., 1991. LAGFD-WAM numerical wave model-I. Basic physical model. Acta Oceanol. Sin. 10 (4), 483–488.
Zelenke, B., O'Connor, C., Barker, C., Beegle-Krause, C.J., Eclipse, L., 2012. General NOAA Operational Modeling Environment (GNOME) Technical Documentation. U.S. Dept. of Commerce, NOAA Technical Memorandum NOS OR&R 40. Emergency Response Division, NOAA, Seattle, WA 105 pp. http://response.restoration.noaa.gov/gnome_manual.
Zheng, L., Yapa, P.D., 1998. Simulation of oil spills from underwater accidents II: model verification. J. Hydraul. Res. 36, 117–134.
Zheng, L., Yapa, P.D., 2000. Buoyant velocity of spherical and non-spherical bubbles/droplets. J. Hydrol. Eng. 126 (11), 852–854. https://doi.org/10.1061/(ASCE)0733-9429.
Zheng, W., Wei, H., Wang, Z., Zeng, X., Meng, J., Ek, M., Mitchell, K., Derber, J., 2012. Improvement of daytime land surface skin temperature over arid regions in the NCEP GFS model and its impact on satellite data assimilation. J. Geophys. Res. 117 (D06117). https://doi.org/10.1029/2011JD015901.